Reprinted from

Symposium on

Machine Processing of

Remotely Sensed Data

June 21 - 23, 1977

The Laboratory for Applications of
Remote Sensing

Purdue University
West Lafayette
Indiana

IEEE Catalog No.
77CH1218-7 MPRSD

APPLICATION OF IMAGE PRINCIPAL COMPONENT TECHNIQUE TO THE GEOLOGICAL STUDY OF A STRUCTURAL BASIN IN CENTRAL SPAIN

ANTONIO SANTISTEBAN
Centro de Investigación UAM-IBM, Universidad Autonóma de Madrid, Spain

LAURA MUNOZ
Catedra de Geodinámica Interna, Universidad Complutense, Madrid, Spain

ABSTRACT

We describe a method to obtain the principal components of a multispectral image. It allows a simultaneous radiometric enhancement by means of a suitable finer level quantization that does not introduce artifacts. Using this method we are able to produce good photographic prints of the principal components of LANDSAT MSS images. As a matter of fact the two first components (that we call bands A and B) alone contain nearly all the information existing on the original image while the other contain only noise.

We use this technique to help in the geological study of Campo Arañuelo Basin, in Central Spain aimed to confirm the hypothesis of different geological histories since Miocene times of this area and the remainder of Tajo Basin.

I. INTRODUCTION

Multispectral remote sensors provide data in the form of several spectral images of the observed area, each one representing the spatial distribution of the reflected light of frequencies lying in the corresponding spectral windows. Therefore rather high correlations are to be expected between these spectral images of the *same* area. The actual degree of correlation depends on the complexity of the imaged area that usually increases with the resolution of the sensor, on the widths of the spectral windows and on the amount and nature of the noise existing in the data.

LANDSAT MSS images (those we are mostly concerned with) have four rather wide spectral bands (0.1 μm of wavelength width in bands 4, 5 and 6 and 0.3 μm in band 7). Correlations between these bands vary from scene to scene, and even in a given scene considerable variations occur in different subimages. Usual values range from 0.4 to 0.97.

Therefore multispectral images contain a lot of redundant data. In order to reduce them one can choose the less correlated bands. For instance to make colour prints one usually takes three of the bands to be assigned to the three fundamental colours, although in this way redundant data are kept while a certain amount of information is lost. Something similar happens when one supplies the less correlated bands to an automatic classifier in order to save computer time.

Instead of doing that, it is more advisable to look for some new and more suitable bands: the so called *principal components* of the image, which are bands with no correlation between them. This is achieved by means of the Karhunen-Loève transformation. These uncorrelated bands, that we shall designate by capital letters (A, B, C and D in LANDSAT MSS images) correspond to the eigenvectors of the interband covariance matrix C, being ordered in eigenvalue decreasing order. Then the first few bands contain nearly all the information existing in the original data while the last ones, that contain nearly only noise, can be disregarded without significant loss of information.

Although band A variance is bigger than the variances of all original bands, it usually needs for radiometric enhancement if we want the image to be photographically recorded for photo-interpretation purposes. Obviously the other bands also are to be radiometrically enhanced. Nevertheless forcing high contrast (specially by means of non-linear radiometric enhancement as for instance the histogram equalization method) implies the introduction of artifacts that sometimes are misleading. To avoid this problem we not only obtain the principal components by means of the orthogonal transformation that diagonalizes C (as it was formerly done by Ready and Wintz[1]) but also can apply a dilatation to perform simultaneously the required radiometric enhancement in such a way that no empty grey levels appear.

Image principal component technique has been used by Fontanel *et al*[2] for a geological study in the South of France. In this paper we discuss this technique from a different point of view and apply it to another geological problem: the study of the structural basin of Campo Arañuelo in Central

Spain. We discuss in Section II the mathematics of our method to obtain the principal components of a n-band multispectral image. In Section III we describe the geological characteristics of Campo Arañuelo basin. Section IV is devoted to the description of the LANDSAT imagery studied and the numerical characteristics of the principal components. Finally we discuss the results in Section V.

II. THE PRINCIPAL COMPONENTS OF A MULTISPECTRAL IMAGE

We are going to study the most general problem of obtaining the principal components of a n-band image, being the intensity levels m-bit numbers, although some of the most significant ones may be always zero, i.e. the actual number of bits may be m'<m. We shall eventually particularize the results to LANDSAT MSS images where n=4, m'=7 for bands 4, 5 and 6 as they are delivered by NASA and m'=6 for band 7, and we take m=8 as usual.

Let us consider a pixel as an element $\vec{x}$ of the n-dimensional vector space on the real numbers R^n, being its intensity levels in the n bands, x_i, $i=1,\ldots,n$, its coordinates in a given orthonormal base $\{\vec{e}_i,\ i=1,\ldots,n\}$. Therefore

$$\vec{x} = \sum_{i=1}^{n} x_i \vec{e}_i$$

As a matter of fact pixels are very special vectors because their coordinates in the base $\{\vec{e}_i\}$ are restricted to be m-bit integers, i.e.

$$x_i \in J_m \equiv \{\chi \mid \chi \in Z \subset R,\ 0 \le \chi \le 2^m - 1\},\ i=1,\ldots,n$$

During the following calculation we allow pixels to take values on R and only on the final step we will approximate them by elements of J_m.

Let us consider the n-band image as a vector random variable $\vec{X}$ on the space of events R^n. Its coordinates in the base $\{\vec{e}_i\}$ are the random variables X_i, $i=1,\ldots,n$ that correspond to the n original image bands. The variance of $\vec{X}$, i.e. the covariance matrix of its coordinates, is

$$C = E\left([\vec{X}-E(\vec{X}) \otimes \vec{X}-E(\vec{X})]\right)$$

where E stands for expectation and $\otimes$ denotes tensor product. C is a symmetric matrix, therefore it can be diagonalized. Let λ_i, $i=1,\ldots,n$ be its eigenvalues, i.e. the roots of the secular equation

$$|C-\lambda 1| = 0$$

(1 being the unit matrix) in decreasing order

$$\lambda_1 > \lambda_2 \ldots > \lambda_n$$

We assume, for the sake of calculation simplicity, that there are no degenerate eigenvalues, although this assumption is not essential. Let $\{\vec{g}_i,\ i=1,\ldots,n\}$ be the orthonormal base formed by the eigenvectors of C that satisfy the equations

$$C\vec{g}_i = \lambda_i \vec{g}_i,\ i=1,\ldots,n$$

and G the orthogonal matrix that diagonalizes C:

$$GCG^{-1} = \Lambda,$$

where

$$\Lambda_{ij} = \lambda_i \delta_{ij},\ i,j=1,\ldots,n$$

The rows of G are the eigenvectors of C, i.e.:

$$G_{ij} = (\vec{g}_i)_j,\ i,j=1,\ldots,n$$

The random variables

$$Y_i = \sum_{j=1}^{n} G_{ij} X_j,\ i=1,\ldots,n$$

are the coordinates of $\vec{X}$ in the base $\{\vec{g}_i\}$. These variables are uncorrelated provided that their covariance matrix is Λ. Only if the probability distribution of $\vec{X}$ were normal, would the new random variables be independent instead of being simply uncorrelated.

The coordinates of the vector $\vec{x}$ in the base $\{\vec{g}_i\}$, i.e. the intensity levels of the pixel in the uncorrelated bands, are

$$y_i = \sum_{j=1}^{n} G_{ij} x_j,\ i=1,\ldots,n$$

These numbers do not belong to J_m. Therefore we finally define the intensity levels of the pixel in the principal components of the image as

$$z_i = \begin{cases} 0 & \text{if } a_i y_i + b_i \le 0 \\ \text{Int}\ (a_i y_i + b_i) & \text{if } 0 \le a_i y_i + b_i \le 2^m - 1 \\ 2^{m-1} & \text{if } 2^m - 1 \le a_i y_i + b_i \end{cases} \qquad (1)$$

where Int stands for integer value and a_i, b_i, $i=1,\ldots,n$ are parameters to be determined. Obviously $z_i \in J_m$, $i=1,\ldots,n$ although a suitable selection of the parameters a_i, b_i, $i=1,\ldots,n$ must be done in order to obtain meaningful results. Linear transformations have no effect on the correlation between the new bands, therefore the covariance matrix of the principal components is approximately

$$a_i a_j \Lambda_{ij},\ i,j=1,\ldots,n$$

being the small actual differences due to the round-off error and tail cut-offs introduced by (1).

Equation (1) allows us to radiometrically enhance the image principal components at the same time that they are obtained. We consider the following four criteria to determine a_i, $i=1,\ldots,n$

being always

$$b_i = \frac{2^m-1}{2} - a_i E(Y_i)$$

$$= \frac{2^m-1}{2} - a_i \sum_{j=1}^{n} G_{ij} E(X_j),\ i=1,\ldots,n$$

in order to center the probability distributions of z_i, i=1,...,n on the mid-point of the interval $[0,\ 2^m-1]$.

1. Take

$$a_i = \frac{1}{\sqrt{n}},\ i=1,\ldots,n$$

in order to reduce the maximum possible length of the interval on which y_i can take values (i.e. the length of the diagonal of the n-dimensional hypercube) to 2^m-1.

2. Apply a radiometric enhancement with the same gain for all bands.

$$a_i = \frac{2^m-1}{2\alpha\sqrt{\lambda_1}},\ i=1,\ldots,n$$

being α a parameter to be determined depending on the enhancement wanted. Hence the standard deviation of band A (the first principal component) is $(2^m-1)/2\alpha$ while the standard deviations of the other bands decrease proportionally to the corresponding eigenvalues of C.

3. Apply different radiometric enhancements to all bands with

$$a_i = \frac{2^m-1}{2\alpha\sqrt{\lambda_i}},\ i=1,\ldots,n$$

in order for all bands to have standard deviations $(2^m-1)/2\alpha$.

4. Omit the shrinkage of option 1 taking

$$a_i = 1,\ i=1,\ldots,n$$

This choice is more advisable than option 1 when the intensity levels of the original bands cover only a fraction of the interval $[0,\ 2^m-1]$.

Options 2 and 3 produce a finer level quantization and an artificial increase of variance. The difference between a photographic print of an image produced through options 2 or 3 and other print produced through options 1 or 4 followed by a radiometric enhancement is that the former has all levels occupied and then no artifacts are introduced although it looks something smoother. In option 2 the relative information contents of all principal components is maintained while in option 3 the bands with smaller variances are more stretched.

On the other hand since G is a orthogonal matrix it is evident that

$$\sum_{i=1}^{n} C_{ii} = \sum_{i=1}^{n} \lambda_i$$

Then the reduction of a multispectral image to its principal components implies a redistribution of variance. If we define the entropy function (see [3])

$$H(C) = -\sum_{i=1}^{n} \pi_i \log \pi_i$$

where

$$\pi_i = \frac{C_{ii}}{\sum_{j=1}^{n} C_{jj}},\ i=1,\ldots,n$$

it can be shown that the minimum of this function is $H(\Lambda)$, obtained when we use the principal components. Therefore the variances λ_i, i=1,...,n are a certain measure of the information contents of each component and it can be shown[1] that, assuming that the noise on the image data is white the improvement in the signal to noise ratio in band A with reference to the original band is

$$\Delta_i = \lambda_1 / C_{ii},\ i=1,\ldots,n \qquad (2)$$

All these formulae can be streightforwardly applied to LANDSAT MSS images. In particular option 4 can be used without any cut-off taking place because their bands have at most 7-bit data while the principal components have 8 bits.

Our computer program to obtain the principal components of a 4-band image (written in FORTRAN IV and IBM system 360 assembler language) uses a very fast algorithm to calculate the covariance matrix that only needs 5 register-to-register multiplications to compute the contribution of each pixel to the 10 different elements of that matrix. It requires 78K bytes of main storage and takes 9 minutes 45 seconds of CPU time in an IBM 360/65 computer to calculate the covariance matrix of a whole LANDSAT MSS image (7.6×10^6 pixels). i.e 77μsec per pixel. To construct the four new bands it needs 108K byte of main storage and takes additional 19 minutes 25 seconds of CPU time, i.e. 153μsec per pixel. This program has been included in the Earth Resources Management interactive system ER-MAN II (formerly ERIPS).

III. DESCRIPTION OF THE AREA STUDIED

The area that we are going to study is the Campo Arañuelo Tertiary Basin[4], West end of the Tajo Structural Basin in Central Spain. It includes parts of the provinces of Toledo and Cáceres.

The rocks forming the borders of the basin, that we will refer to as *the basement* regarding to their dynamic behaviour during the most recent movements, are mainly granite and metamorphic rocks of Paleozoic age that have been fractured

since Hercynian orogeny. In Alpine movements they behaved like a rigid unit and constituted the source-areas providing the sediments for filling the basin. These sediments are mainly arkoses and conglomerates with arkosic matrix, probably of Oligocene age. We will refer to them as the *sedimentary mantle*. The activity of the numerous faults located in the basement-sedimentary mantle contact has enhanced the habitual topographic contrast between these materials. Among the fault and fracture trends existing in the basement as a heritage of Paleozoic orogenies, only those between NNE-SSW and NE-SW show up clearly the effects of a recent reactivation.

The expected goal of a global study of this area is to draw some conclusions about the geological history of the whole Tajo Basin in order to confirm the geological individuality of Campo Arañuelo Basin in post-Oligocene times with respect to the rest of Tajo Basin, in agreement with the existence of a conjectured crustal megastructure in Central Spain[5]. This megastructure, a oval-shaped uplift whose major axis follows an approximate NE-SW trend, happens to be divided in two halves for an E-W fault zone and this fact involves smaller activity in the southern half, in which Campo Arañuelo Basin is located, than in the other half during the Middle and Younger Tertiary era.

IV. THE LANDSAT IMAGERY USED

In order to study Campo Arañuelo Basin we have considered four LANDSAT MSS scenes. Two of them (2333-15404 of 21st December 1975 and 2350-10175 of 7th January 1976) were taken during the winter with very low sun elevation angle (20° in both). In them the fault-block mountains conforming the Northern boundary of the basin happen to be covered by snow, hence all their faults and ice-modeled geomorphological features are hidden. The non-snow-covered topographic forms are enhanced by the shadowing produced at low sun elevation angles, therefore this images give us good geological information provided that the dynamic processes have been very recent and then the correlation between structures and topographic landforms is still high (deep gorges, flat-iron facets and other features involving a youthful stage of evolution are common in this area). Nevertheless due to the low ilumination rock-type discrimination by tonal differences is extremely difficult even on the contrasted materials outcropping in this area.

Conversely in a summer image (scene 2170-10201 of 11th July 1975) with high sun elevation angle (58°) rock-type discrimination by tonal differences is much easier while topographic forms are very difficult to see.

Then we decided to use scene 1228-10325 of 8th March 1973 for its intermediate sun elevation angle (37°) that allows rather good rock-type discrimination by tonal differences and also shows up topographic forms.

This image had been geometrically corrected using 14 ground control points and interpolated by means of the nearest neighbour algorithm[6] in order to have pixels corresponding to squares of 50.8 m of side on the ground. From this geometrically corrected image we have selected a subimage of 1560 pixels of width by 917 pixels of length that represents an area of 79.2 Km by 46.6 Km on the provinces of Cáceres and Toledo (in Central Spain) around Navalmoral de la Mata, including all Campo Arañuelo region. Table 1 gives the parameters that characterize the probability distribution of pixel radiometric levels in the four original bands.

Table 1. Statistical parameters of the probability distributions of radiometric levels in the original bands of Campo Arañuelo subimage.

Band	Mean	Standard Deviation
4	15.13	3.81
5	22.05	5.78
6	36.53	9.08
7	20.41	5.66

The covariance matrix of the Campo Arañuelo subimage is

$$C = \begin{pmatrix} 14.51 & 20.54 & 22.19 & 10.87 \\ 20.54 & 33.43 & 30.89 & 14.40 \\ 22.19 & 30.89 & 82.38 & 49.40 \\ 10.87 & 14.40 & 49.40 & 32.04 \end{pmatrix}$$

The correlation matrix, defined by

$$\rho_{ij} = \frac{C_{ij}}{\sqrt{C_{ii} C_{jj}}}, \quad i,j=1,\ldots,4$$

is then

$$\rho = \begin{pmatrix} 1. & 0.933 & 0.642 & 0.504 \\ 0.933 & 1. & 0.589 & 0.440 \\ 0.642 & 0.589 & 1. & 0.962 \\ 0.504 & 0.440 & 0.962 & 1. \end{pmatrix}$$

Therefore in this subimage the most correlated bands are the two near infrared bands and the two visible bands, while the correlation between one visible and one infrared bands is much smaller. Nevertheless even the smallest correlation (0.440 between bands 5 and 7) is relatively high. The eigenvalues of C are:

$$\lambda_1=132.95,\ \lambda_2=27.05,\ \lambda_3=1.27,\ \lambda_4=1.09,$$

and its eigenvectors are

$$\vec{g}_1 = \begin{pmatrix} 0.249 \\ 0.358 \\ 0.775 \\ 0.457 \end{pmatrix} \qquad \vec{g}_2 = \begin{pmatrix} 0.443 \\ 0.770 \\ -0.285 \\ -0.361 \end{pmatrix}$$

$$\vec{g}_3 = \begin{pmatrix} 0.851 \\ -0.521 \\ 0.011 \\ 0.075 \end{pmatrix} \qquad \vec{g}_4 = \begin{pmatrix} 0.135 \\ 0.092 \\ -0.564 \\ 0.809 \end{pmatrix}$$

Table 2 lists the parameters that characterize the probability distributions of the principal components obtained according to option 4 (see Section II). The differences between their variances and the eigenvalues of C due to round-off errors are very small. Band A has 81.9% of the total variance, band B 16.6%, band C 0.8% and band D 0.7%. Therefore bands A and B have 98.5% of the total variance and this is a measure of the amount of information contained in them. These bands are a very good input for an automatic classifier, much better than bands 5 and 7 (the less correlated ones). On the other hand they can also be used (if radiometrically enhanced) to make a two colour composite print very useful for photo-interpretation purposes.

Table 2. Statistical parameters of the probability distribution of radiometric levels in the principal components of Campo Arañuelo subimage obtained through option 4.

Band	Mean	Standard Deviation	Variance
A	127.00	11.53	133.01
B	127.00	5.21	27.13
C	127.01	1.17	1.36
D	126.99	1.08	1.17

We use equation (2) in order to have an estimate of the signal to noise ratio improvement achieved by means of band A, although stripping (the most important noise component) is not white noise. The values of Δ_i are: 2.1 dB with respect to band 6 (the one with the highest variance) and 9.6 dB, 6.0 dB and 6.2 dB respectively with respect to the more frequently used bands 4, 5 and 7.

As we pointed out before rather than apply a contrast enhancement to the principal components obtained through option 4, in order to photographically record them we prefer to use option 3. Good results are obtained with α between 2.0 and 3.0. We conventionally take α=2.65 because in normal probability distributions the fraction of pixels accumulated on the grey levels 0 and 255 as a consequence of the tail cut-offs is approximately 1/256.

The values of the gain factors applied are:

$$a_1=4.17, \quad a_2=9.25, \quad a_3=42.66, \quad a_4=46.13.$$

Figures 1 and 2 show respectively bands A and B obtained in this way. Photographs have been produced by means of a DICOMED D-47 film recorder. We have added at the botton right part of the photographs a grey wedge with 17 levels (16×k, k=0,1,...,15 and 255); it can be used as a test of the quality of the prints and also provides a scale reference because their lenght corresponds to 25.9 Km on the image. We do not include prints of bands C and D because they contain nearly only noise.

Band A appears free from stripping. Band B shows some stripping on the water bodies. This is a consequence of the poor quality of original data As a matter of fact detector miscalibrations are such that the mean values of the data gathered over the whole frame by two of the sensors of band 4 differ in 1.4 radiometric levels while the differences between the standard deviations are 0.9. When we deal with better original images, band B happens to be also strippingless[7].

V. CONCLUSIONS

Prior to any LANDSAT data analysis a regional survey was done. It included field rock identification, fault measurement and mapping. Attention was not paid to any geological feature due to older-than-Tertiary processes in the basement rocks. We are interested only in the recent geological history of the area and this has to be obtained by the study of the sediments, their facies, spacial location related to the source-areas, etc. We realized that the sedimentary mantle includes a wide range of detritic rocks and lacks of the Young-Tertiary gypsum and limestone units so thickly accumulated on the rest of Tajo Basin.

We concluded that the materials have had a short transportation from the source-areas provided the high angularity showed by both quartz and feldspar detritic particles. The deduced dynamic conditions are those corresponding to a pulsational rising of the old faulted blocks in the source areas, starting this reactivation in the Older-Oligocene and lasting until the end of this period. This non-continuous rising involved discontinuous detritic accumulation in the basin, as the numerous cross-beddings, broken layers and lenticular rock-bodies prove. These minor preliminary movements finished with a major dynamic phase that ended the sedimentary process and moved the old-generated reverse faults located in the basement limit[8], the Paleozoic materials getting on top of the Tertiary layers just deposited. We can assume that the Tertiary dynamic history of this area ended at that time, while in the rest of the Tajo Basin it extended further producing complete Miocene series. The Eastern limit of Campo Arañuelo Basin is determined by a basement faulted block in the area of Talavera de la Reina that gives rise to a step in the deep sedimentary basin floor not only detectable by means of stratigraphic and hydro-geological research but also noticeable in LANDSAT images.

LANDSAT imagery helped us in the global study of Campo Arañuelo Basin by its ability to show up major geological features as regional scale

faults, folds and basin boundaries and to facilitate rock-unit mapping.

Band A (see Fig. 1) is very good for differentiation of materials and not so good for the visualization of faulted structures. On the other hand band B (see Fig. 2) turns out to be nearly useless for geological purposes, but it shows up clearly man-made features as highways, railroads and towns. It also allows good vegetation differentiation.

It is easy to differenciate between the basement and sedimentary mantle rock-types by means of band A. It also allows the discrimination between Paleozoic and Tertiary rocks as well as among Paleozoic rocks themselves. Some differentiation between the types of the granites that form the Northern boundary of the basin is also feasible. Conversely a Tertiary facies classification is not possible because of the qualities inherent to the sediments that also make impossible this classification by means of high-altitude aircraft photography, and that even make it very difficult in the field work.

The SE-NW folds are clearly visualized (see the schematic map of Fig. 3) while the contact delineation between granite and metamorphic rocks is very difficult. It may be a consequence of denudation differences: while the quartzite-schists layers in the folds give rise to topographic forms that are very easy to detect on LANDSAT images, there is no landforms in the granite-metamorphic rocks contact because of denudation uniformity.

Fractures and faults are better visualized on the Northern boundary of the basin than on the Southern one. From this fact we can deduce an asymmetry between these two areas, with a larger block-rising process in the Northern part. This conclusion is in agreement with the hypothesis of the Central Spain megastructure[1] (see Section III) according to which the movements of the Southern boundary of Campo Arañuelo Basin have been just a dynamic reflection of those of the Northern one.

ACKNOWLEDGEMENTS

Thanks are given to the Instituto Geográfico y Catastral for the photographic recording and development of the pictures.

REFERENCES

1. Ready, P.J., and Wintz, P.A., "Information Extraction, SNR Improvement, and Data Compresion in Multispectral Imagery", *IEEE Trans. on Communications* COM 21, 1123 (1973).

2. Fontanel, A., Blanchet, C., and Lallemand, C., "Enhancement of Landsat Imagery by Combination of Multispectral Classification and Principal Component Analysis" *Proc. of the NASA Earth Resources Survey Symposium* vol. I-B p. 991 (Houston, 1975).

3. Wantanabe, S., "The Loève-Karhunen Expansion as a Means of Information Compresion for Classification of Continuous Signals", IBM Tech. Rep. AMRL-TR-65-114 (1965).

4. Hernández-Pacheco, F., "Rasgos Fisiográficos y Geológicos de la Vera, del Tramo Medio del Valle del Tiétar y del Campo Arañuelo", *Bol. R. Soc. Esp. Hist. Nat.* 48, 217 (1950).

5. Alía, M., "Una Megaestructura de la Meseta Ibérica: La Bóveda Castellano-Extremeña" *Estudios Geol.* 32, 229 (1976).

6. Bernstein, R., "Digital Image Processing of Earth Observation Sensor Data" *IBM J. Res. Dev.* 20, 40 (1976).

7. Santisteban, A., "Determination of Uncorrelated Bands in a LANDSAT MSS image", *Thematic Mapping Land Use, Geological Structure and Water Resources in Central Spain. Project no. 28760. Final Report*, p. 93, (Instituto Geográfico y Catastral, Madrid 1976).

8. Martín Escorza, C., "Actividad Tectónica, Durante el Mioceno, de las Fracturas del Basamento de la Fosa del Tajo" *Estudios Geol.* 32, 509 (1976).

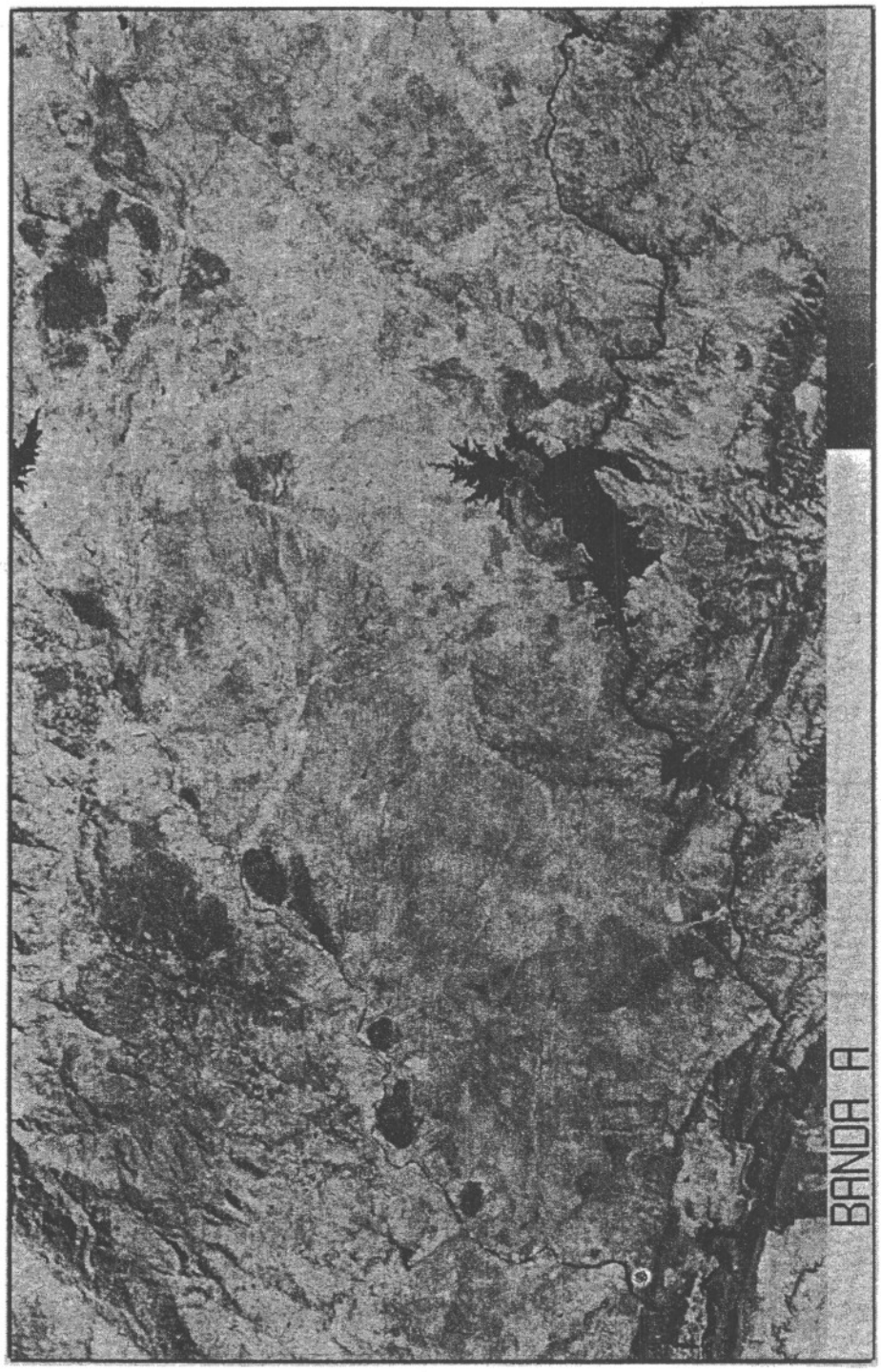

Figure 1. Band A of Campo Arañuelo image obtained through option 3.

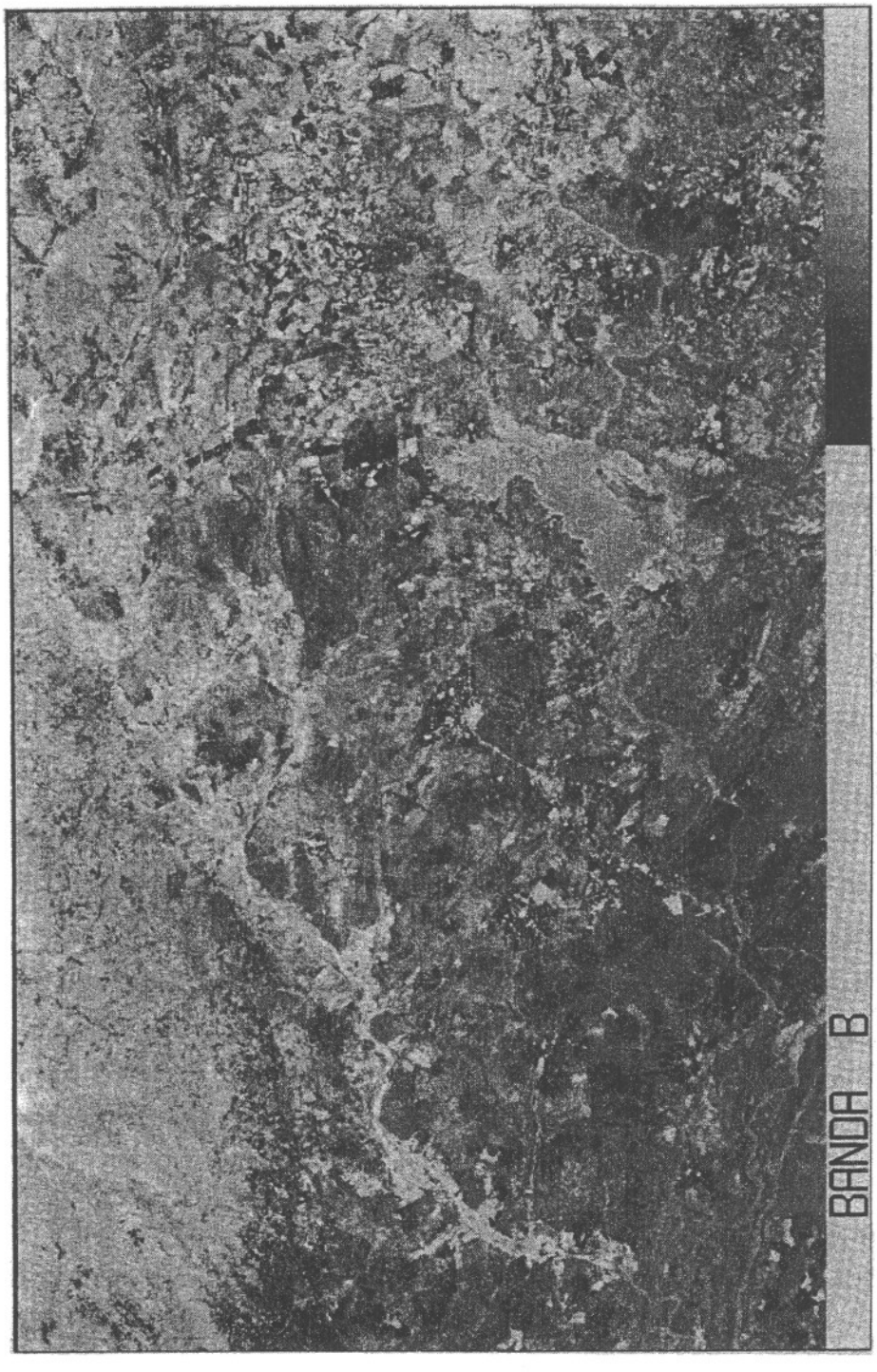

Figure 2. Band B of Campo Arañuelo image obtained through option 3.

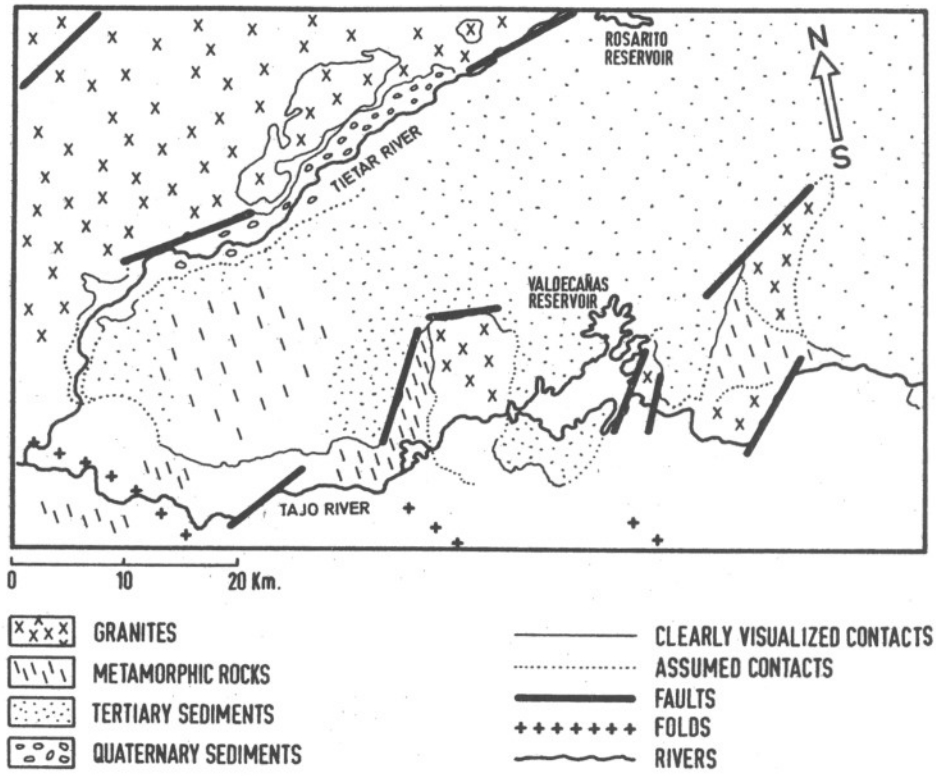

Figure 3. Photointerpretation of band A of Campo Arañuelo image.

Antonio SANTISTEBAN. Born in Santander in 1947. Studied Physics in Madrid at the Universidad Complutense (formerly Universidad de Madrid) and obtained the degrees of Licenciado (1969) and Doctor (1974). Worked on Theoretical Elementary Particle Physics (1969-75). Has been Assistant Teacher of Quantum Mechanics (1969-74) and Assistant Professor of Applied Mathematics (1974-75) at the Department of Theoretical Physics of the same University. Since 1973 works in the IBM Madrid Scientific Center at the Universidad Autónoma de Madrid on Image Processing applied to Remote Sensing.

Laura MUÑOZ. Born in Navalmoral de la Mata (Cáceres) in 1953. Studied Geology in Madrid at the Universidad Complutense (formerly Universidad de Madrid) and obtained the degree of Licenciado in 1975. Is a postgraduate student at the Department of Internal Geodynamics of the same University.